

Explicit Incorporation of Prior Anatomical Information Into a Nonrigid Registration of Thoracic and Abdominal CT and 18-FDG Whole-Body Emission PET Images

Oscar Camara*, Gaspar Delso, *Member, IEEE*, Olivier Colliot, Antonio Moreno-Ingelmo, and Isabelle Bloch, *Member, IEEE*

Abstract—The aim of this paper is to develop a registration methodology in order to combine anatomical and functional information provided by thoracic/abdominal computed tomography (CT) and whole-body positron emission tomography (PET) images. The proposed procedure is based on the incorporation of prior anatomical information in an intensity-based nonrigid registration algorithm. This incorporation is achieved in an explicit way, initializing the intensity-based registration stage with the solution obtained by a nonrigid registration of corresponding anatomical structures. A segmentation algorithm based on a hierarchically ordered set of anatomy-specific rules is used to obtain anatomical structures in CT and emission PET scans. Nonrigid deformations are modeled in both registration stages by means of free-form deformations, the optimization of the control points being achieved by means of an original vector field-based approach instead of the classical gradient-based techniques, considerably reducing the computational time of the structure registration stage. We have applied the proposed methodology to 38 sets of images (33 provided by standalone machines and five by hybrid systems) and an assessment protocol has been developed to furnish a qualitative evaluation of the algorithm performance.

Index Terms—Anatomical constraints, free-form deformations (FFD), nonrigid registration, oncology, thoracic and abdominal computed tomography (CT), whole-body positron emission tomography (PET).

I. INTRODUCTION

THE combination of anatomical and functional information provided by computed tomography (CT) and positron emission tomography (PET) imaging modalities can have a

Manuscript received June 16, 2006; revised October 27, 2006. This work was supported by the French Ministry for Research under Grant 01B0267. *Asterisk indicates corresponding author.*

*O. Camara was with the TSI Department, Ecole Nationale Supérieure des Télécommunications, CNRS UMR 5141, Paris, France. He is now with Centre for Medical Image Computing, Department of Medical Physics, University College London, London WC1E 6BT, U.K (e-mail: o.camara-rey@ucl.ac.uk).

G. Delso was with the TSI Department, Ecole Nationale Supérieure des Télécommunications, CNRS UMR 5141, Paris, France. He is now with Medical Imaging Systems Group, Philips Medical Systems, 92156 Suresnes Cedex, France (e-mail: gaspar.delso@philips.com).

O. Colliot was with the TSI Department, Ecole Nationale Supérieure des Télécommunications, CNRS UMR 5141, Paris, France. He is now with CNRS, UPR 640 LENA, Cognitive Neuroscience and Brain Imaging Laboratory, Université Pierre et Marie Curie–Paris 6, Hôpital de la Pitié-Salpêtrière, Paris, France (e-mail: olivier.colliot@chups.jussieu.fr).

A. Moreno-Ingelmo and I. Bloch are with the TSI Department, Ecole Nationale Supérieure des Télécommunications, CNRS UMR 5141, Paris, France (e-mail: antonio.moreno@enst.fr; isabelle.bloch@enst.fr).

Color versions of one or more of the figures in this paper are available online at <http://ieeexplore.ieee.org>.

Digital Object Identifier 10.1109/TMI.2006.889712

significant impact [1] on improving medical decisions for diagnosis, staging, planning, radiotherapy, or monitoring. On the one hand, PET scans provide valuable knowledge about metabolic abnormalities, but give limited information on the anatomy around the increased uptake, making precise lesion localization quite difficult. On the other hand, CT is not as sensitive as PET but offers accurate anatomic detail, pinpointing the exact size, shape, and location of diseased tissue. The benefit of the combination of these complementary imaging modalities has been proven in a large number of clinical studies. An extensive review of these works can be found in [2].

Nevertheless, integrating data from these imaging modalities is a challenging task, in particular in thoracic and abdominal images. One needs to compensate for the elastic nature of the organs located in these regions, the large intrasubject variability in terms of motion, anatomy and metabolic activity and the different physical nature underlying both acquisition techniques, in order to achieve the combination of both types of information. All these factors add up to cause displacements of up to 10 cm between corresponding structures. For instance, Goerres *et al.* [3] found a maximum of displacement of 8.29 cm in the diaphragm between a PET scan and a CT image acquired at maximum inspiration. Until few years ago, physicians visually integrated information provided by CT and PET scans acquired in separated devices, using their anatomical knowledge and expertise to identify homologous points between the images. Unsurprisingly, this procedure was very rough and time-consuming, and uncertainty in the mapping from one image to another could lead to uncertainty in clinical decisions.

The development of combined PET-CT systems, introduced by scanner constructors in the late 1990s [4] represented a huge step towards an automatic solution of this problem. These machines allow the acquisition of anatomical and functional information in the same session and device, thus furnishing a hardware (or mechanical) integration. Nevertheless, these systems cannot deal with physiological motions between CT and PET acquisitions due to breathing, cardiac cycle or insufficient patient cooperation [3]. Several studies [5]–[8] have proven the presence of artifacts in images acquired with combined PET-CT machines in the lungs and the liver, mostly due to respiration.

Before the introduction of PET-CT combined machines, software-based registration techniques were the only way to compensate for differences between images acquired with

standalone devices. Nowadays, such algorithms can also be used to cope with physiological-induced deformations between images acquired with hybrid systems. Some complete reviews on registration methods can be found in [9]–[13]. Several works have been published in the context of thoracic and abdominal CT-PET registration. A study of the role of image registration in nuclear medicine was published by Hutton *et al.* [14]. Some of these registration techniques [15]–[19] employed linear (rigid or affine) transformations in these regions. However, linear transformations being unable to compensate deformations due to normal metabolic activity, some authors have moved forward to nonrigid registration algorithms. Sato *et al.* [20] proposed a point-to-point matching methodology based on a Cauchy–Navier spline transformation. The main drawback of this method is the high computational cost associated to the optimization of the cost function. Meyer *et al.* [21] applied a mutual information-based algorithm in thoracic CT-PET and abdominal computed tomography single photon emission computed tomography (CT-SPECT) registration applications, using a full affine mapping and a five-point thin-plate spline (TPS) warped registration technique. The major drawback of this method is the manual selection of the control points required for the TPS model. A similar method was proposed by Slomka *et al.* [22], which is based on the extraction of corresponding control points from the lungs and the application of a TPS interpolation algorithm from the corresponding control points that furnishes a dense nonrigid transformation. The main drawback of this approach concerns the selection of the control points. For instance, when working with images having tumors within the lungs, the ray-tracing technique will find control points in the tumor rather than in the lung contours. Furthermore, there is a lack of information in the regions far away from lungs and body contours (even information within the structures is not taken into account). Tai *et al.* [23] have developed and evaluated a nonrigid CT and whole-body PET registration method using transmission PET scans. Erdi *et al.* [24] also employed the transmission PET image to guide the registration with the CT image in a thoracic application.

One elegant solution to the registration of chest CT and transmission PET images was proposed by Mattes *et al.* [25], in which deformations were modelled with a B -spline FFD transformation and using mutual information (MI) as the similarity measure. The authors pointed out that obtained results were not completely satisfactory on more deformable regions such as the diaphragm or the abdomen. Based on Mattes' work, Delzescaux *et al.* [26] studied the influence of the CT respiration phase and the free-form deformation (FFD) model ability to cope with nonlinear deformations due to respiration movements. They proposed to transform the CT image instead of the PET one in order to preserve the metabolic information provided by functional images, this approach being well-suited for radiotherapy applications. Carlsen and Wischmann [27] also proposed a FFD-based procedure using a CT-derived pseudo-transmission image to compute a nonrigid transformation based on tricubic B -splines. Recently, Shekhar *et al.* [28] proposed a MI-guided elastic registration technique based on multiple rigid-body registrations. They have applied their methodology to a set of images acquired with both standalone and combined machines,

obtaining a registration accuracy comparable to interexpert difference in landmark identification.

All previous nonrigid techniques (except those ones proposed by Sato [20] and Shekhar [28]) assumed a linear relation, or even no deformations, between emission and transmission PET scans. This assumption is not always satisfied because emission and transmission images are not acquired in a simultaneous way. Apart from little differences that can appear in cardiac regions, the main danger of this assumption concerns pathologies or tumors that are only visible in emission PET images. If only the transmission PET scan is used to guide the registration process, tumors will not be taken into account. Furthermore, the liver may not be distinguishable from the surrounding structures in transmission PET scans, therefore, these methods cannot be used in abdominal registration applications. With respect to previous FFD-based registration techniques, none of them directly work on emission PET scans due to their low-SNR quality and the lack of constraints on the FFD transformation model. When working with emission PET images, these approaches tend to get trapped in local minima of the chosen similarity criterion if they are not initialized within a relatively narrow range near to the final solution.

In order to avoid these problems, one can introduce in the registration procedure prior information about the anatomical structures involved in the application. The incorporation of prior anatomical information in registration processes is at the core of current state-of-the-art research in nonrigid registration.

In the majority of cases, prior anatomical information is introduced in an *implicit* way. This approach forces the registration procedure to furnish plausible deformations that have been found by modeling the expected structure variability and the spatial relationships between these structures. Biomechanical finite element models (FEMs) such as the NURBS-based cardiac-torso (NCAT) phantom [29], [30] and statistical model methods such as the active appearance modeling (AAM) [31], the statistical deformation modeling (SDM) [32], or the statistical shape models proposed by Wang and Staib [33] can be used to obtain this prior knowledge. Two major drawbacks are associated to this approach in the context of our application. First, relying on anatomical atlases or expected structure morphology and movements seems too risky when working with pathological images due to the large interpatient variability. Tumors may appear anywhere in the image, considerably modifying the shape and volume of structures, as well as the spatial relationships between them. Secondly, implicit approaches ask for additional registration processes in order to align prior anatomical models to the image data. The main consequence is an increase of the computational overhead of the whole procedure, which is a critical point in our application.

Therefore, we propose a faster approach based on an *explicit* incorporation of anatomical prior information into the registration procedure. Some authors [34]–[37] have presented different ways of merging this anatomical prior information provided by some recognized features in the image with information provided by the whole set of grey-level intensities. Our approach consists in obtaining anatomical knowledge directly from the images to register, making use of a novel hierarchical segmentation technique, and computing a nonrigid transformation be-

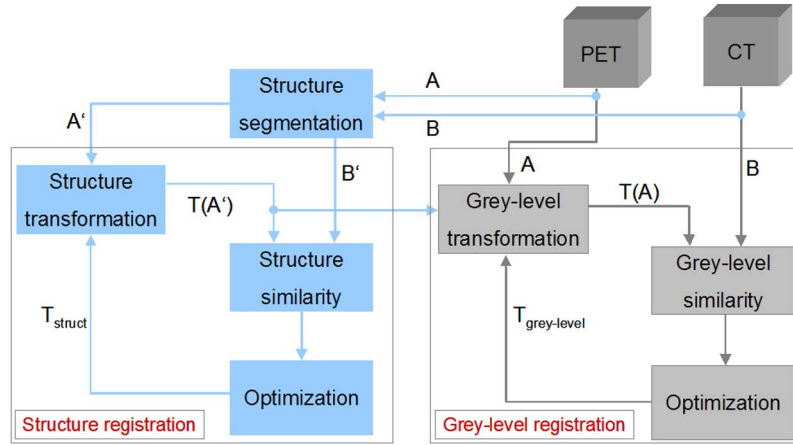


Fig. 1. General scheme of the proposed approach. Left part corresponds to the structure registration stage and the right part to the grey-level registration stage. Transformation obtained between the segmented structures initializes the registration phase that works with the whole set of intensities.

tween the corresponding segmented structures. This information is used to initialize deformations as close as possible to the final solution before applying whole-content registration techniques. With this initialization, the search of the global solution will be constrained and the algorithm will converge in a more robust and faster way. This approach does not make any assumption on the structures themselves or on their deformations, relying only on available information in the images and on a set of robust spatial relationships between the structures, permitting to work with almost any kind of unexpected situations. Moreover, the extraction of anatomical knowledge from the images is in general less expensive in terms of computational cost than registration procedures. The segmentation of corresponding structures in CT and emission PET images is achieved by means of a hierarchical segmentation method based on the mathematical modeling of robust spatial relationships between the targeted structures. Nonrigid deformations are modeled in both registration stages by means of FFD, but the optimization of the control points is achieved by an original vector field-based approach, called gradient vector flow-free-form deformations (GVF-FFD), instead of the classical gradient-based technique, considerably reducing (13 times faster) the computational time of the structure registration stage. We have applied the proposed methodology to 38 sets of images, 33 provided by standalone machines and 5 by hybrid systems. A visual assessment protocol has been developed to furnish a qualitative evaluation of the algorithm performance.

The paper is organized as follows. A general scheme of the proposed methodology is presented in Section II. Section III is devoted to the structure segmentation stage and the subsequent nonrigid registration stage applied on the segmented anatomical features is detailed in Section IV. The whole-content registration phase is presented in Section V. In Section VI, we describe the evaluation protocol developed to assess in a qualitative way the accuracy of the registration results. Finally, results are shown in Section VII and conclusions are given in Section VIII.

II. GENERAL SCHEME

A general scheme of the proposed registration methodology is shown in Fig. 1. It is divided into two stages: a structure regis-

tration phase (left part of Fig. 1) in which homologous structures (A' and B') are extracted from both CT and PET images (A and B) and nonrigidly registered; and a grey-level registration phase (right part of Fig. 1) in which a nonrigid registration based on their full intensity content is applied to the original images (A and B). The second stage, initialized with the transformation (T_{struct}) provided by the structure registration stage, furnishes the final nonrigid transformation ($T_{\text{grey-level}}$).

In fact, the structure registration phase can be seen as the first step in an anatomical multiresolution procedure, first extracting from the data and processing the main anatomical structures, then transferring the result as an initial estimate to a higher level where finer anatomical detail is considered. Therefore, the grey-level registration phase can be considered as a refinement step of the structure registration results, capable of correcting errors the segmentation might have induced and improving the registration in those regions distant from the segmented structures.

The use of this strategy also implies a less expensive registration procedure in terms of computational cost, the reasons being the robustness improvement of the registration algorithm in the presence of local minima, and the reduction of the number of iterations required for the grey-level registration phase, due to the proximity of the initial transformation to the final solution.

III. STRUCTURE SEGMENTATION

Our registration methodology requires a set of homologous structures that can be robustly located in both thoracic/abdominal emission PET and CT images. Based on discussions with medical experts, we finally chose to segment the following structures: skin, skeleton¹, lungs, kidneys, and liver. Obtaining an accurate, fully automatic segmentation of the mentioned anatomical structures would be on itself a formidable task, in particular for functional images. Fortunately, segmentation accuracy is not a priority in this application since, in the proposed registration procedure, segmentation errors will not be propagated to the final registration result. The point is that if more

¹The skeleton is only segmented in CT since its extraction with enough robustness in emission PET scans is difficult. Therefore, the skeleton is only used at the CT image segmentation stage as a support structure, but it does not play any role in the registration procedure.

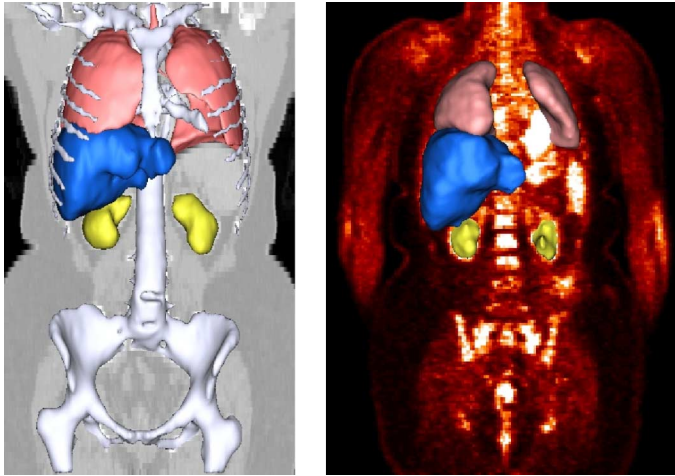


Fig. 2. Meshes of final segmented structures, including skeleton (white), lungs (red), kidneys (yellow), and liver (blue). Left: Rendering of CT segmented structures superimposed on a 2-D coronal grey-level slice. Right: 3-D rendering of PET segmented structures superimposed on a 2-D coronal grey-level slice.

organs are detected, then results are better because we have more constraints over the whole volume. But the segmentation of these organs does not need to be very accurate. Typically, segmentation errors of a few millimeters are not critical in our method. Indeed the second intensity-based, registration stage will be able to correct them. In summary, the quantity of information is important, but its accuracy is not. Therefore, the segmentation procedure will focus on speed and reliability rather than accuracy.

For the segmentation of the targeted structures, relying only on their grey-level intensities proved to be an insufficiently robust strategy, as they depend too much on the acquisition characteristics and suffer from a high inter-patient variability. Consequently, we decided to introduce higher-level information by exploiting the spatial relationships between organs, less sensitive to the deformations than shape and less acquisition-dependent than grey-level values. A hierarchical segmentation procedure has been proposed [38], based on the mathematical modeling of robust spatial relationships between the targeted structures to provide *prior* constraints that will be combined with information from the images. Detailing this method is outside the scope of this paper and the reader can refer to [38] for a complete description of the segmentation procedure. A similar strategy has been successfully used for the segmentation of internal brain structures [39]. An example of structure segmentation results in both CT and emission PET images is shown in Fig. 2, where meshes of final segmented structures, including skeleton, lungs, kidneys and liver, are superimposed on two-dimensional (2-D) coronal slices of CT and emission PET grey-level scans.

The proposed method has been positively evaluated by medical experts, in all CT and PET structures. Lung segmentation results are very accurate in CT images, obtaining subvoxel segmentation accuracy, while some errors (small enough for not inducing final misregistrations due to the grey-level registration stage of the proposed methodology) appear in emission PET scans due to the low SNR of these images. The liver is the most difficult structure to segment in both CT and PET images due

to the presence of neighboring structures with similar grey-level values, such as the heart and aorta artery. Nevertheless, a reasonable approximation of the liver is obtained, notably separating it from the kidneys and the heart. On the other hand, we have often found (around 50% of the cases) small structures close to the liver that our segmentation procedure classifies as false positive liver voxels.

Finally, a retrospective segmentation evaluation based on the assessment of final registration results has also been performed. This has been used to verify that inaccuracies in the segmentation procedure stay within the capture range of the final grey-level registration, and can thus be corrected.

IV. STRUCTURE REGISTRATION

The main goal of this stage is to find a transformation between homologous CT and PET anatomical structures (lungs, kidneys, liver) that have been recognized in the previous segmentation phase. The registration method in this phase works with labeled images (a different label is affected to each three-dimensional (3-D) surface) and it must estimate the deformation between corresponding 3-D structures representing segmented thoracic and abdominal regions.

In our application, the registration procedure must be able to deal with structures having different characteristics in terms of geometry, local regularity and even topology (even if they have in general spherical topology). For instance, the algorithm must deal with the concavities caused by the bronchia in the CT lungs, which are seldom visible in PET; or the kidneys, fairly large, and smooth structures in CT but very crude in PET. Thus, the registration cannot impose severe regularity constraints.

First, an affine registration technique (see Section IV-A) is applied to the extracted homologous structures. Afterwards, a FFD-based registration technique (see Section IV-B), provides a nonrigid transformation between the CT and emission PET anatomical features.

Note that, when registering segmented images with nonrigid techniques such as the ones proposed in this paper, structures could locally slide along their interfaces without this being reflected in the registration similarity measure. Such effect, limited only by the regularity constraints imposed on the transformation, could lead to erroneous registration results. However, this is not a concern in the proposed implementation since the refined registration stage uses the whole content information and does not rely on interfaces anymore. This introduces additional constraints on the registration, which is then able to cope with all possible movements of structures.

A. Affine Registration

In general, nonrigid registration methods compute an initial rigid or affine transformation in order to cope with global deformations between the images to register. In the developed procedure, the segmented structures can be easily used to automatically establish a first approximation of the alignment. This includes translation and scaling in the three axes and cropping out the parts of the volumes without a correspondence or that have no interest for our application. This is achieved using a computed bounding box surrounding the structures to register

in both modalities. Trivial as it may seem, this simple step allows the whole system to be independent of the actual field-of-view (FOV) of the original images, unlike classical registration methods which need a prior manual adjustment (mainly in the z direction, as in [40]). Thus, once bounding boxes are built, translation and scale are already roughly recovered just by annotating the appropriate change in image origin position and voxel size. Then, we apply a classical affine registration technique [41] between CT and PET bounding boxes, using Powell's multidimensional direction set method [42] in order to refine the parameters of the affine transformation.

B. GVF-FFD

Nowadays, there is a large number of different nonrigid registration methods available in the literature, mainly differing in the transformation models used to compensate the deformations between the features to register. In our opinion, three of these models are particularly interesting for our application: those based on radial basis functions (RBFs), fluid methods, and FFD.

Radial basis functions [43], [44], formulate the transformation as a linear combination of kernel functions such as Thin-Plate [45] or Clamped-Plate [46] Splines. In general, registration methods based on RBF use anatomical features detected in both images as homologous control points. Then, after mapping each control point in the source image to its homologous in the target, the RBF are used to interpolate the control point displacements to create a dense mapping between both images. An interesting characteristic of these techniques is that there are no geometry restrictions to the control point distribution, i.e., it can be sparse and irregular. On the other hand, numerous and well-distributed control points in the image are required in order to assure acceptable registration results when the deformations are very local or do not respond to the inherent physical model. However, the selection of these control points in a simple and robust way remains a difficult problem, especially in emission PET images, and we would not be able to provide a large enough set of corresponding references adequately distributed all over the data volumes. Furthermore, as the range of each control point is not necessarily local, if the number of control points is elevated this technique is very expensive in computational terms.

Fluid-based techniques [47]–[49] are based on physical laws that provide an unconstrained model in which the source image is modeled as a viscous fluid which gradually deforms over time to match the target image. Such techniques have too many degrees of freedom for our purposes, being computationally expensive and inadequate to be applied in applications involving noisy imaging modalities such as PET.

FFD based techniques, introduced by Sederberg *et al.* [50], are a particular case of FEMs (which have been firstly used by Gee *et al.* [51] for medical image registration purposes) based on radial basis functions that has known an important success in the field of computer graphics. First used by Rueckert *et al.* [52] for medical image registration purposes, they model the transformation as a linear combination of spline basis functions. In this technique, deformations of the object volume are achieved by tuning an underlying mesh of control points but, unlike other RBF, FFD make use of a regularly distributed grid of control

points, the position of these being independent of the underlying image (grid points no longer need to be homologous anatomical references), thus avoiding the control point selection phase. Some authors [53], [54] have compared the performance of fluid and FFD registration algorithms, concluding that FFD furnish slightly better or equivalent results to the fluid ones. The use of cubic B -splines to interpolate the displacements of the control point grid guarantees that moving any control point will only have a local effect on the image, significantly reducing the computational cost associated to its optimization.

Therefore, a nonrigid transformation based on B -spline FFD has been chosen to compensate the deformations involved in our application.

1) *Gradient-Based Optimization*: In this technique, deformations of the source volume (the PET scan in our application) are achieved by tuning a regular mesh of control points (ϕ being an uniformly spaced grid of $n_x \times n_y \times n_z$ control points $\phi_{i,j,k}$ with a spacing of δ and i, j, k being the indices within the grid). The spacing δ between the control points of the FFD grid has been chosen according to the magnitude of the local deformations and the resolution and the size of the images to register. We have empirically set the distance between control points to 20 mm, which has proven to provide accurate enough results.

In general, the optimization of the transformation parameters (i.e., control point displacements, $\phi_{i,j,k}$) is achieved by applying iteratively a gradient descent technique to all control points simultaneously [52], advancing along the gradient direction until no further improvement of the similarity measure is found. This gradient estimation is performed by computing local differences over the control point grid. This procedure is embedded in a multistep framework (the initial optimization step μ is divided by 2 at each level), in order to cope first with severe deformations and progressively take finer ones into account.

In addition, a local spring force regularization term has been included, pulling each node towards the centroid of its neighboring nodes, in order to avoid overfitting and to prevent the control point grid from autointersecting, which could lead to unwanted alterations of the structure topology. This force has been defined heuristically and, despite not strictly forbidding intersections, it has been observed to perform well, provided the optimization step is small with respect to node separation.

An advantage of working with labelled images is that a simple and robust criterion such as the root mean square (rms) can be used as the similarity measure that will guide the registration (rms-FFD) of the segmented structures. Some tests have been conducted using more sophisticated measures such as the label consistency, proposed by Rueckert *et al.* [55], but without substantial improvements in the results.

2) *Vector Field-Based Optimization*: An important drawback of the classical optimization method described above is its high computational burden. This is due to the nature of the optimization procedure, in which a local gradient estimation is needed at each iteration to update the control point displacements of the whole grid. For instance, in a grid of 10 nodes per dimension, the algorithm must compute at each iteration the gradient for 3000 parameters. Multiresolution and multigrid approaches accelerate the convergence of the algorithm, but the gradient estimation remains a problem in terms of computation time.

We have proposed [56] a novel approach to speedup the optimization of the control point displacements, using a 3-D vector field v computed using the contours of segmented target structures (in our case, CT structures) instead of the gradient-based procedure employed in the rms-FFD algorithm. This vector field provides at each image voxel a displacement vector tangent to a smooth path towards the nearest structure. Making the image evolve along these paths will generally assure a good matching.

Therefore, at each iteration m , we update the displacement of every control point in the FFD grid according to the information provided by the displacement vectors located in its neighborhood

$$\phi_{i,j,k}^{m+1} = \phi_{i,j,k}^m + \mu \frac{1}{R} \sum_{r=0}^R p_{r,i,j,k} v_r \quad (1)$$

where R denotes the number of source structure contour points under the influence of a given control point and $p_{r,i,j,k}$ is a weight based on the distance between the contour and the control points. The mean of the resulting vectors is taken as the optimal control point displacement direction. The magnitude of the displacement also depends on the step (μ) of the optimization procedure. At the end of each iteration, a local spring regularization term is applied to prevent the control point grid from autointersecting.

The convergence of the algorithm depends on the quality of the computed vector field v . In order to avoid undesirable oscillations around the target contour, a precomputed distance map is checked at the end of each iteration and used as a stop criterion. The multistep framework also helps reducing this problem by dealing with large deformations in the first iterations and with more local ones at the end.

The main advantage of this approach is that the vector field v is computed only once at the beginning of the procedure, unlike the gradient estimation that must be updated at each iteration. Moreover, as only the voxels belonging to the structure contours are scanned, the computational burden of the algorithm is substantially reduced. Algorithm 1 summarizes the proposed control point optimization procedure.

Algorithm 1 Optimization of control point displacements with a 3-D dense vector field

```

for all segmented structures to register do
  contour detection of the structures to match {already affinely registered}
  computation of  $v$  over target structure contours
  While  $\mu \neq \mu_{\text{end}}$  do
    While  $\text{distance}(n) \leq \text{distance}(n - 1)$  do
      for all control points do
        computation of  $r$ 
        store  $v$  values of  $r$  (i.e.,  $v_r$ ) and weight them with the distance with respect to the control point ( $p_{r,i,j,k}$ )
        update control point displacement with (1)

```

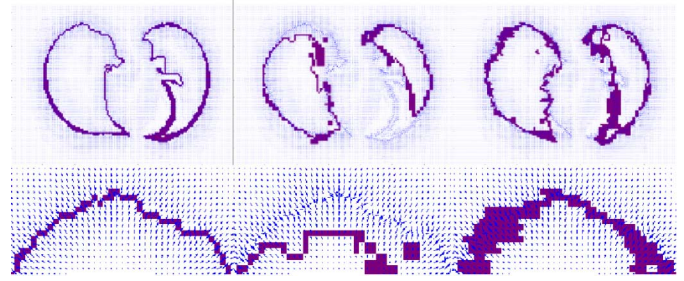


Fig. 3. Evolution of PET lung contours towards their corresponding CT ones using the GVF-FFD method. A 2-D axial slice of the GVF field derived from the CT contours is superimposed on them (left), on the PET contours before (center), and after (right) evolution. Top: 2-D axial slice. Bottom: detail.

```

end for

```

```

application of local spring regularization term

```

```

apply FFD grid to source structure contours

```

```

computation of the distance between target and source contours

```

```

end while

```

```

divide  $\mu$  by 2

```

```

end while

```

```

end for

```

The simplest way to obtain v would be to make use of a vector distance transform technique computed on CT structure contours. An alternative can be the use of the gradient vector flow (GVF) technique [57], that is usually employed to guide deformable models in segmentation applications. The advantage of the GVF with respect to the vector distance transform approach is the presence of a regularization term controlling the trade-off between the smoothness of the vector field and the fidelity to the contour gradients of the image. A smooth vector field is better suited for optimizing FFD control points in order to avoid local minima, at the expense of slightly increasing the computational cost of the algorithm due to the regularization term.

The left part of Fig. 3 shows a 2-D axial slice of the superimposition of CT lung contours on the GVF field computed over them. It can be observed that despite the regularization term, the local irregularities of the lungs are well coped with. An example of the evolution of PET lung contours towards their corresponding CT contours is also shown in Fig. 3. We can appreciate the remarkable improvement of the contour match after applying the GVF-FFD registration method (right in Fig. 3) with respect to results obtained by a rigid registration procedure (center in Fig. 3).

It must be pointed out that in our registration context, in which we need to register several thoracic and abdominal structures at the same time, some problems could arise if noncorresponding structures overlap since the labels are not taken into account in the contour evolution. We deal with this situation by computing the GVF field and making the source contours for each structure evolve independently. Therefore, at the end of the structure

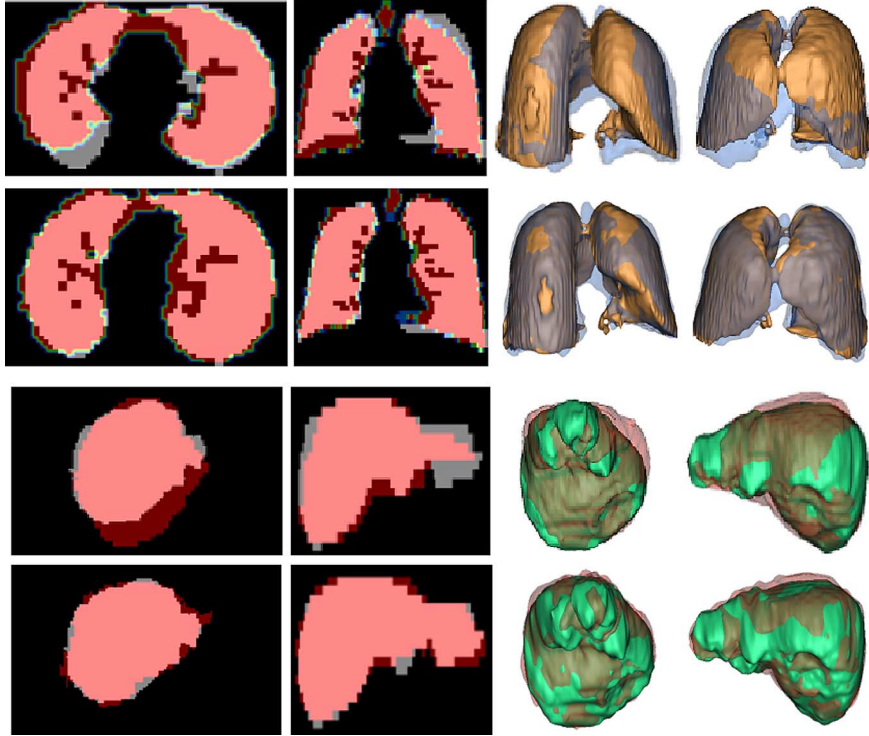


Fig. 4. Structure registration results obtained with the GVF-FFD method. Left part of the figure: 2-D coronal and axial slices of CT (grey) segmented lungs (top rows) and liver (bottom rows) are superimposed on their homologous PET structures (red), registered with a rigid transformation (first and third row) and with the GVF-FFD method (second and fourth row). Right part of the figure: a 3-D representation of the same structures is shown (CT lungs in blue, registered PET lungs in brown, CT liver in green, and registered PET liver in red).

registration procedure, an average of the displacements is taken for those control points affected by more than one structure.

C. Evaluation of Structure Registration Methods

Examples of results obtained by registering PET segmented structures (lungs and liver) with their homologous in CT images using the GVF-FFD and affine registration methods are displayed in Fig. 4. On the left part of the figure, 2-D axial and coronal slices of superimposed CT (grey) and registered PET (red) structures are shown. In a similar way, two different views of the superimposition of the 3-D CT (blue for CT lungs and green for CT liver) and registered PET (brown for registered PET lungs and red for registered PET liver) rendered structures are also shown.

We have computed three different registration measures between target and registered structures, aiming at comparing the performance of the affine, rms-FFD and GVF-FFD structure registration techniques. Let T and F be the set of voxels corresponding to the target and the registered source structures, respectively, and let the operator $|A|$ be the cardinality of the set of voxels A . The three criteria [58] used for estimating structure registration accuracy are the following:

$$\begin{aligned}
 \text{OM} &= \frac{|T \cap F|}{|T \cup F|} \\
 \text{SENS} &= \frac{|T \cap F|}{|T|} \\
 \text{SPEC} &= \frac{|T \cap F|}{|F|}
 \end{aligned} \tag{2}$$

where OM is the Jaccard overlap measure, SENS the sensitivity, and SPEC the specificity.

The overlap measure (OM) is a classical criterion to evaluate the matching between two structures and consists of the quotient between intersection and union of structures to evaluate, which is equal to 1 if total overlap (best registration) is achieved. The sensitivity (SENS) and specificity (SPEC) measures give us additional information about how the overlap of both structures is achieved. For instance, if the registration of two structures yields a low sensitivity value but a high specificity one, it means that the registered source structure is too small. Both criteria are also equal to 1 if total overlap is achieved. It must be pointed out that the registered source must be thresholded at 50% of the nonzero label value of the structures in order to avoid an overestimation of the computed measures. In order to avoid this thresholding phase, the set of fuzzy overlap measures recently proposed by Crum *et al.* [59] could be used.

Both nonrigid structure registration methods have been applied to a database composed of 20 pairs of deformable structures (13 lungs and seven livers). These structures have been obtained applying the segmentation procedure described in [38] to CT and PET images of the same patient (eight cases) and using the NCAT phantom [29], [30] to generate structures at different stages of the respiratory and cardiac cycles (12 pairs of structures).

Table I summarizes the results (mean value \pm standard deviation) furnished by the quantitative assessment measures computed on the whole set of registered structure pairs. Whereas rms-FFD technique provides the most accurate registration results, the GVF-FFD method still clearly surpasses the affine reg-

TABLE I
EVALUATION OF STRUCTURE REGISTRATION METHODS. OM: OVERLAP MEASURE. SENS: SENSITIVITY. SPEC: SPECIFICITY.
VALUES CORRESPONDING TO THESE MEASURES REPRESENT THE MEAN AND THE STANDARD DEVIATION OF THESE MEASURES

	Lungs			Liver		
	OM	SENS	SPEC	OM	SENS	SPEC
Affine	0.731 ± 0.129	0.831 ± 0.171	0.869 ± 0.039	0.820 ± 0.034	0.893 ± 0.026	0.909 ± 0.033
RMS-FFD	0.857 ± 0.037	0.996 ± 0.003	0.860 ± 0.035	0.902 ± 0.006	0.998 ± 0.001	0.904 ± 0.006
GVF-FFD	0.821 ± 0.065	0.956 ± 0.048	0.852 ± 0.038	0.876 ± 0.016	0.987 ± 0.014	0.886 ± 0.006

istration technique. The three evaluated methods provide more accurate results in the liver than the lungs, and in a similar way, they perform slightly better with data coming from the NCAT phantom than from CT and PET derived structures. It is worth mentioning that differences between segmented structures coming from real CT and PET data are usually larger than those from the NCAT phantom, and that lung registration is more challenging than liver due to the presence of large surface irregularities to deal with. Sensitivity and specificity measures are close to 1 for both FFD-based methods, with specificity values slightly lower, proving that, in general, the registered source structure remains smaller than the target one. On the contrary, the affine method produces objects overpassing target structure sizes. Furthermore, we observe that differences of registration accuracy between results provided by the rms-FFD and GVF-FFD are larger in structures undergoing more local deformations such as the lungs. These effects are due to the tradeoff in the computation of the GVF vector field between the rejection of outliers and the capacity to cope with local deformations.

In addition to the registration accuracy measures, the convergence times of each structure registration method have been analyzed due to its major significance in our application. All values have been normalized by the dimensions of the images, so performances can be compared independently of image size. As expected, the GVF-FFD method shows much better performances (52.610 μ s/voxel) than the rms-FFD technique (699.365 μ s/voxel), i.e., around 13 times faster.

In consequence, the choice between the rms-FFD and GVF-FFD techniques will depend on the priorities for a given application, concerning registration accuracy or low computational costs. It has already been mentioned that, in the proposed method, the posterior grey-level registration phase will complement the structure registration stage, thus at this point only an approximation of the transformation between the structures to register is needed. Therefore, we prefer to use the GVF-FFD technique due to the good trade-off between its convergence times and the registration accuracy it provides. Nevertheless, if better registration accuracy were needed for a given application, the GVF-FFD technique could be used as a starting point, switching to rms-FFD to refine the results.

V. GREY-LEVEL REGISTRATION

The grey-level based registration phase is the last stage of the proposed registration methodology. This stage aims at refining registration results provided by the initial structure registration phase computed on segmented thoracic and abdominal structures. Furthermore, it must furnish a displacement field

for regions far away from the segmented structures and even within them because at this point, reliable registration information based on their own characteristics (mostly grey-level values) has not yet been taken into account. For instance, this stage must provide a complete registration information corresponding to the ventricles of the heart, since the only information available up to this point came from the registration of the mediastinal wall, as the heart ventricles were not taken into account in the structure registration stage. Finally, another objective of this stage is the correction of misregistrations that may have been introduced by structure segmentation errors, taking advantage of the entire image grey-level information we are now working with.

This grey-level registration stage is essentially the method proposed by Rueckert *et al.* [52] in a nonrigid registration of contrast-enhanced breast magnetic resonance imaging (MRI) application. The nonrigid transformation is modeled by a FFD based on B -splines using normalized mutual information (NMI) as a similarity measure. This approach has been successfully used in several registration applications involving different imaging modalities [25], [32], [60], [61]. Nevertheless, the lack of constraints on the FFD model, the lack of uptake of several structures and the low SNR quality in the emission PET scans impede the straight use of this methodology in our application. In fact, this technique tends to converge towards local minima of the similarity criterion unless a very accurate initialization is provided. Fig. 5 shows a registration result obtained when applying a FFD-based registration technique without constraints between a pair of CT and emission PET scans of the same patient acquired with standalone machines.

We can observe in the nonrigidly registered emission PET image (bottom right in Fig. 5) that the FFD-based registration technique fails to provide acceptable results. For instance, we can observe that several critical structures are fully misregistered such as the liver or the kidneys and that the lung registration is not accurate enough. The set of intensities in emission PET scans corresponding to the boundaries of these structures are not well distinguished and, depending on the incremental step in the parameter optimization stage and the number of multigrid and multiresolution levels, some incorrect transformations can provide good similarity measure values. These parameters must be large enough to cope with severe deformations involved in these nonrigid regions, but the lack of constraints in the FFD model allowing any possible correspondence between the images produces these misregistrations. The tuning of the registration parameters could improve these results as well as the use of multigrid techniques, but we consider that, even if

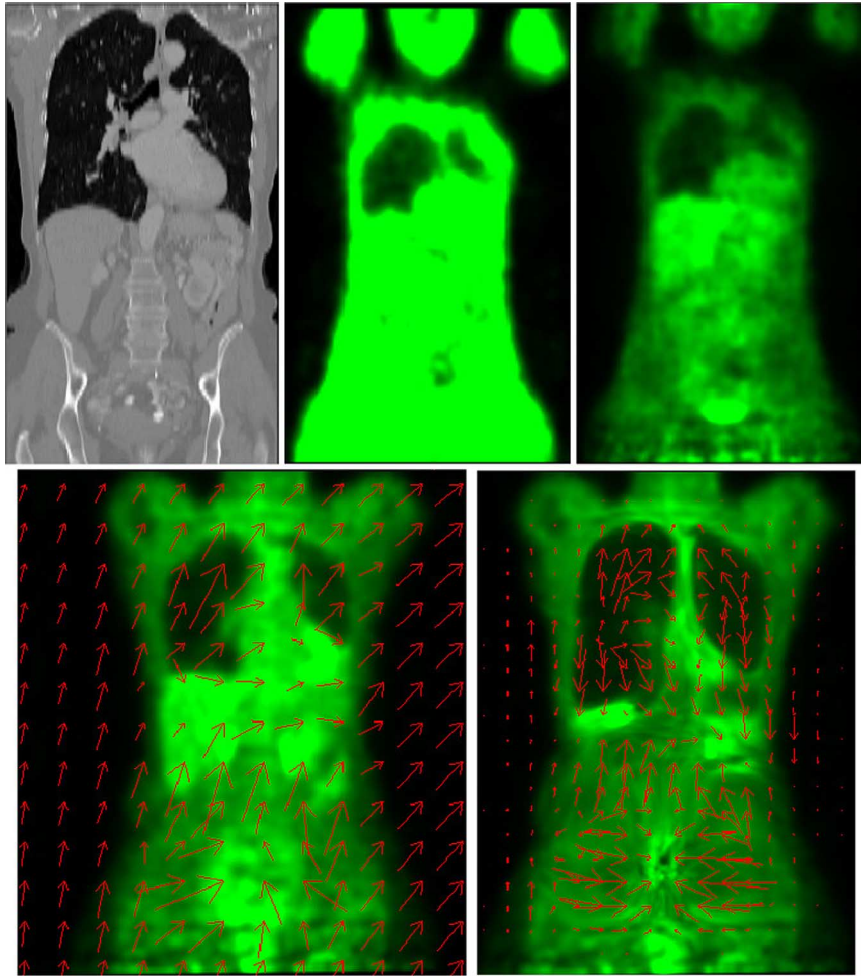


Fig. 5. Results obtained by computing an affine + FFD transformation without constraints between CT and emission PET images. Top: CT (left), transmission (center), and emission PET (right) original images. Bottom: registered emission PET images obtained by applying affine (left) and affine + FFD (right) transformations. Displacement field (red arrows) associated to each one of these transformations (affine on the left and FFD on the right) is superimposed on the images.

this NMI-FFD registration technique has been proven to be successful in some applications, it must be modified in order to deal with CT and emission PET images. For these reasons, in the proposed registration methodology, an accurate initialization is provided by the structure registration stage, furnishing to the NMI-FFD approach an initial transformation very close to the final solution, at least in the neighborhood of the segmented structures.

Furthermore, the inclusion of the previous initial structure registration phase allows us to skip some of the lower multiresolution steps of the time-consuming fine registration, thus substantially speeding up the overall process. The average computational time was around 2 h (the range goes from 50 min to 3 h), around 20 min corresponding to the segmentation and structure registration stages, in a Linux condor cluster (one CPU per registration) when applying the proposed registration methodology, thus reducing by an order of three the time needed for the FFD registration technique without constraints. It is difficult to compare these computational costs with other published in the literature in other medical imaging applications due to the influence of the image sizes and resolutions, the image quality, the nature of the deformations to cope with, the number of degrees

of freedom in the transformation model or the available computational power. Nevertheless, just for giving a reference, Crum *et al.* [53] stated that fluid and B -spline FFD techniques took between 2 h and 10 h per registration in an intersubject brain registration application working with MR images. Considering that in our application processed images are larger, the fact that the poor image quality of PET images could easily make the algorithm converge towards local minima and the larger deformations we need to cope with, we think that results obtained by the proposed methodology in terms of computational cost are meritorious.

VI. EVALUATION

Evaluating the result accuracy of a nonrigid registration method is a complex problem both conceptually and in practice. Indeed, nonrigid motions are difficult to perceive in three dimensions, and it must be checked that the registration algorithm corrects deformations in mobile structures while not introducing new errors in the more stable ones. This problem is aggravated in our application due to the lack of gold standard since manual segmentations in emission PET images will not be reliable enough to assess either a segmentation or a registration

procedure. Furthermore, even combined PET-CT scanners are unable to furnish a perfectly registered image that could be used as a reference for assessing nonrigid registration methods.

A. Visual Assessment Protocol

Even if it is a semi-objective validation technique, visual inspection by medical experts allows in our application to judge and classify, into a scoring scale of error values, registration results for the most important anatomical structures. Mattes *et al.* [25] have employed this approach to evaluate the registration accuracy of a nonrigid approach applied on chest CT and transmission PET images. We present a similar visual assessment protocol² that allows physicians and registration specialists to rapidly generate a semiobjective and qualitative measure of the registration accuracy, being repetitive enough to allow statistical interpretation of the results.

For this purpose, several anatomically significant 2-D slices of both the original CT and registered emission PET volumes, are presented. Slices have been evenly spaced through the volume in order to display the most significant thoracic and abdominal structures. For example, for a $256 \times 256 \times 97$ volume, six coronal and six axial slices are employed. This is performed by means of an automatic procedure that uses CT segmented structures in order to decide which 2-D slices must be chosen for evaluation purposes. However, the user has also access to all 2-D axial slices of the CT and the registered emission PET volume if they must be checked in order to confirm any evaluation score. Furthermore, the user has the possibility of changing the display intensity range settings of the 2-D slices.

Each pair of 2-D slices has been marked with a ruler that defines some reference or landmark points as it crosses significant anatomical structures, such as the chest wall (ribcage), the mediastinal wall (heart), the diaphragmatic wall (liver), or the stomach and kidneys walls. These references allow the user to estimate differences in the position of the mentioned structures in both 2-D slices and then score the registration accuracy of the method. For instance, in the case of the lungs, the user must evaluate the registration result accuracy in the anterior, posterior, inferior, and superior part of both, left and right lungs. Fig. 6 shows one pair of these 2-D slices, corresponding to axial (top) and coronal (bottom) slices.

This procedure is certainly limited in the sense that the evaluation only measures local translation errors at the reference points that are placed on the surface of some structures, and no assessment about registration result accuracy in other regions or even within the evaluated structures is provided. In general, an expert user needs about 20–30 min to complete the validation process, thus considerably faster than Mattes' evaluation interface [25].

The scoring (or dissatisfaction) scale has been defined by medical specialists keeping in mind that the goal of the registration method was to attain errors below the resolution of PET images (in general, voxel dimensions of PET images are around $4.0 \times 4.0 \times 4.0 \text{ mm}^3$ in our database). Table II shows the scale and its correspondences in millimeters and in pixels.

²It has been developed under the supervision of Dr. H. Foehrenbach, from the H. I. A. Val de Grâce, Paris, France.

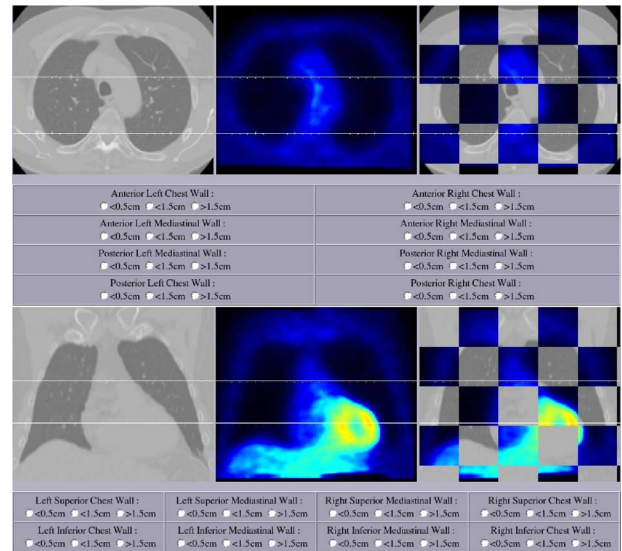


Fig. 6. Example of 2-D axial (top) and coronal (bottom) slices of the CT (left), registered PET (center) volumes, and the chessboard display (right) used in the visual assessment protocol. They are marked with the rulers (white) that define landmark points where registrations must be evaluated.

TABLE II
EVALUATION SCORING SCALE

Score	mm	Pixels	Quality
0	0-5	0-1	Good
1	5-15	1-3	Acceptable
2	15-	3-	Unacceptable

We have estimated the interobserver consistency of the developed visual assessment protocol in order to verify if it is repetitive and objective enough to be used for the evaluation of registration algorithms. A group of three clinicians of three different clinical centres, all of them with a strong experience in oncology, have used the developed evaluation protocol in order to assess registration result accuracy furnished by the proposed methodology.

The evaluation procedure has been used by these physicians in an independent way and assessment results have been sent back by means of the developed online *html* web form. They have assessed five registration thoracic and/or abdominal cases selected from the available database, each one with different degrees of registration accuracy, for the estimation of the interobserver consistency. The number of landmark points in which the registration has been assessed was: 208 for the lungs; 20 for the kidneys; 36 for the liver; 22 for the heart; and 10 for the stomach.

In order to have an estimation of the interobserver consistency for each targeted region, we have computed the percentage of landmark points in which the three evaluators have scored the registration accuracy with the same score; only two of the evaluators have agreed with the same score; or when the three evaluators do not agree at all. Obtained results are summarized in Fig. 7. We can appreciate a good performance of the proposed visual assessment protocol in all the targeted structures in terms

TABLE III
VISUAL ASSESSMENT PROTOCOL RESULTS. STRUCT: STRUCTURE REGISTRATION. FINAL: GREY-LEVEL REGISTRATION.
RMS: RMS-FFD INITIALIZATION METHOD. GVF: GVF-FFD INITIALIZATION METHOD

	Score = 0 (%)				Score = 1 (%)				Score = 2 (%)			
	Struct		Final		Struct		Final		Struct		Final	
	RMS	GVF	RMS	GVF	RMS	GVF	RMS	GVF	RMS	GVF	RMS	GVF
Lungs	60.63	54.25	72.04	71.15	28.70	34.32	19.48	20.43	10.67	11.43	8.48	8.42
Heart	62.90	58.36	70.63	70.93	31.08	35.27	24.62	23.55	6.02	6.37	4.75	5.52
Liver	55.83	51.88	65.41	66.54	35.03	37.58	27.05	26.19	9.14	10.54	7.54	7.27
Kidneys	77.50	78.22	77.50	77.71	20.83	20.11	20.83	20.62	1.67	1.67	1.67	1.67
Stomach	33.19	31.12	41.09	39.15	18.79	20.37	21.30	22.17	48.02	48.51	37.61	38.68

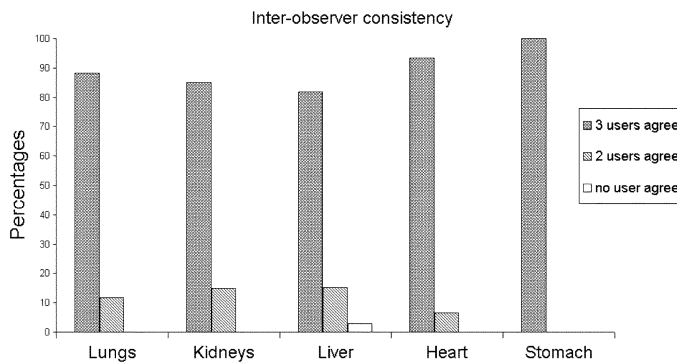


Fig. 7. Interobserver consistency measure.

of inter-observer consistency. All cases in which one evaluator disagrees with the others involve scores differing only in one step of the scoring scale, i.e., from good to acceptable or from acceptable to unacceptable, but never from good to unacceptable. We also observe that there exists more discrepancies for the liver and kidneys than for the lungs. This is due to the presence of several structures in abdominal CT images having similar intensity values. On the other hand, discrepancies in the lungs are mostly due to the lack of strong contours in emission PET images, in particular after applying the nonrigid transformation. An interesting conclusion from Fig. 7 is that the protocol can correctly assess the registration accuracy when it is not satisfactory, such as in the stomach. Finally, it must be pointed out that only in one reference point, the three evaluators have completely disagreed, also proving the appropriateness of the visual assessment protocol.

VII. RESULTS

A. Database and Study Description

During this work, 33 data sets composed of CT, emission and transmission PET scans acquired with standalone machines of thoracic and/or abdominal regions provided by LifeScan Louisville, KY, Centre Hospitalier Universitaire (C.H.U.), Liège, Belgium, Percy Hospital, France, and Hôpital d'Instruction des Armées (H.I.A.) du Val de Grâce, France, have been used. Furthermore, five additional data sets were available from

Centre Hospitalier Princesse Grace (C.H.P.G.) of Monaco and C.H.U. of Liège, acquired with a combined CT-PET machine.

A common problem when using images from different sites is the lack of homogeneity in terms of image quality, due to the use of different scanners and clinical protocols employed to acquire the images. We have designed our registration procedure in order to be as much independent as possible of image acquisition characteristics in order to avoid reformatting our image database to a common standard. Therefore, CT images have a size of 256×256 or 512×512 pixels in the xy plane (axial plane) and between 60 and 125 slices (depending on their FOV, corresponding to a thoracic and/or an abdominal case), with voxel dimensions approximately $1.0 \times 1.0 \times 5.0 \text{ mm}^3$. PET images have a size of 144×144 pixels in the xy plane (axial plane) with 160 to 230 slices, with voxel dimensions around $4.0 \times 4.0 \times 4.0 \text{ mm}^3$.

We have employed the visual assessment protocol on the registration results furnished by the proposed methodology, without comparing them with the ones provided, for instance, by the FFD registration approach without constraints. We consider that, by means of a visual inspection of Fig. 5, one can clearly observe that the absence of anatomical constraints on the FFD registration procedure involves inaccurate results. On the other hand, we have used the evaluation protocol with the images obtained after the structure registration stage, both using the rms-FFD and the GVF-FFD strategies to compare them with the final results and thus to have an estimation of the performance of the grey-level registration stage.

Therefore, the visual assessment protocol has been used by five expert evaluators to assess the 33 different CT and emission PET image registrations coming from standalone machines³, including thoracic and abdominal cases. Results obtained from the visual assessment protocol are summarized in Table III. It shows, for each significant thoracic and abdominal structure, the percentage of landmark points in which the registration error is scored as good, acceptable or unacceptable, according to the scoring scale of Table II.

³We consider that the reduced number of cases acquired with combined machines does not allow to obtain reliable statistics when applying the visual assessment protocol, thus they are just visually evaluated.

B. RMS-FFD Versus GVF-FFD Initialization Methods

Results shown in Table III are similar to those ones obtained in Section IV-C with respect to the performance of the two initialization methods presented in this paper: the GVF-FFD strategy provides less accurate results than the rms-FFD technique. Nevertheless, the grey-level registration stage compensates for these differences, at the expense of a minor addition in computational cost (around 100 min for the rms-FFD and 108 min for the GVF-FFD).

C. Structure Versus Grey-Level Registration

Concerning the comparison between results after the structure and the grey-level registration stages, we can observe a substantial improvement at the end of the procedure for all structures, except the kidneys. This enhancement involves the correction of possible segmentation errors (the lungs and the liver) as well as the fact of taking into account the grey-level information of not-segmented structures (the heart and the stomach). The lack of improvement in the kidneys is due to the good quality of their segmentation (very spherical structures) and the lack of strong deformations on these structures.

D. Stand-Alone Machines

Inspection of Table III illustrates the good performance of the proposed nonrigid registration methodology for the majority of the evaluated regions including lungs, kidneys, liver, and heart. On the other hand, some misregistrations appear near the stomach. These results are slightly better (registration errors under PET voxel size of 4 mm against 5 mm errors) to those ones recently presented by Shekhar *et al.* [28], but this could be due to the different image databases or the evaluation protocols used in both studies. A proper comparison of both registration methodology performances would be very useful to elucidate which one is better suited for this particular application or to combine their respective strengths into a more robust algorithm.

In particular, results obtained in the thoracic wall are very satisfactory, even in the diaphragmatic region where the transformation computation was very critical due to the large deformations suffered in this region. The upper part of both lungs have in all cases small registration errors, while some landmark points corresponding to the lower part of the lungs have a score of 1. The unacceptable errors found in the lungs correspond to the posterior mediastinal wall, due to the large differences in this region between CT and emission PET images.

The proposed registration methodology takes advantage of the proximity of the heart to the lungs and the strong constraints imposed on them to furnish good and acceptable registration errors of the heart.

We can observe that the kidneys produce the lowest registration errors, and this is due to the lack of strong deformations on these structures and their good initialization furnished by the segmentation-based registration stage. Landmark points corresponding to the kidneys that have a score of 2 concern those ones of the right kidney close to the stomach, due to the influence of this structure on their registration. On the other hand, most of the

landmark points corresponding to the left kidney have a score of 0 (even if there are some scores of 1 in zones close to the liver).

The proposed registration methodology provides good and acceptable registration errors in the liver, despite the difficulties of this structure. Its landmark points scored as 0 correspond in general to the upper part and the left wall of the liver, while the ones in which the registration has been scored as 1 are located on the lower part of the liver. Some unacceptable registration errors are found on the right wall of the liver since, sometimes, there are small abdominal structures close and having similar intensity values to the liver that can produce good similarity measure values, even if the registration is not well done.

Most important registration errors have been found in the stomach (it is the only targeted structure having a mean of scores close to 1), due to the severity of its deformations and the lack of strong constraints imposed on this structure. Nevertheless, some good and acceptable scores have been assigned to the landmark points corresponding to the stomach that are relatively close to the kidneys and the lungs because they take advantage of the initialization registration stage applied to these structures.

One final registration result example is shown in Fig. 8. This case is very interesting due to the presence of a malignant tumor located in the left lung. The challenge of the transformation computation between these images is illustrated in the top row of coronal slices in Fig. 8, where it can be easily seen that the tumor is found in distant coronal slices after applying an affine registration transformation to the emission PET image (Fig. 8, top row, center). The application of the proposed nonrigid registration methodology has allowed to obtain a transformation capable of placing the tumor in the correct coronal slice (Fig. 8, top row, right).

Nevertheless, it must be pointed out that the performance of the proposed methodology is not optimal in all pathological cases, strongly depending on the location of the tumor. The majority of problems arise when the tumor is located within a structure suffering strong deformations such as the lungs, since the structure registration applies a transformation to the tumor that does not necessarily correspond to its own movement. On the other hand, as shown in Fig. 8, this situation is no more a problem when the pathology is located close to the edge of a segmented structure. The inclusion of tumors as an additional structure in the segmentation and first registration stages, as detailed in [62], would reduce these problems.

E. Combined Machines

The proposed registration methodology has been also applied to five images acquired with a combined CT-PET system. Minor or no improvement has been visually observed on all but one of the sets of images acquired by a hybrid system when applying the proposed registration methodology. Fig. 9 demonstrates the special case in which there is a substantial improvement on the superimposition of the CT and PET images, located in the cardiac region, after applying our procedure. Nevertheless, it must be pointed out that only five of these pairs of images were available and most of them did not present either substantial visible artifacts or visible tumors, i.e., cases in which a retrospective nonrigid registration algorithm could give additional information to the mechanical registration furnished by these machines.

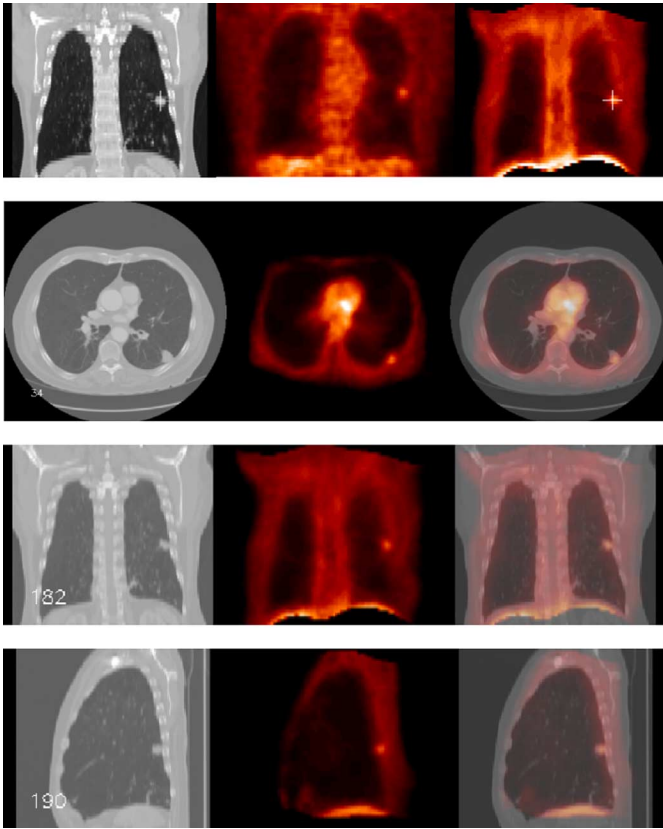


Fig. 8. Final registration result. 2-D coronal slices (top row) of the CT image (left), the emission PET image registered with an affine transformation (center), and the emission PET image registered with the proposed nonrigid registration methodology (right). Mark on the top row points out where the tumor is located. It can be seen that the tumor is found in different coronal slices after applying an affine transformation (center) and that this problem is solved using the proposed nonrigid registration methodology (right). An axial (second row), a coronal (third row), and a sagittal (bottom row) 2-D slices of the CT (left) and the registered emission PET (center) images, and their superimposition (right) are shown.

Therefore, we cannot draw any conclusions about the application of the proposed methodology on these images until a more exhaustive database is available.

VIII. CONCLUSION

We have presented a registration methodology adapted to cope with deformations between CT and emission PET images in order to combine anatomical and functional information provided by these imaging modalities. It is mostly based on the explicit incorporation of prior anatomical information into the registration procedure.

We have visually shown (see Fig. 5) that a FFD registration technique without constraints fails to provide accurate enough results when it is directly applied on the grey-level images. Nevertheless, this model has proved to be a flexible technique allowing us to construct an original registration methodology and providing us a simple way of interaction between the feature-based and intensity-based registration phases. This interaction between these two theoretically confronted methods, derived from the chosen strategy, has allowed us to combine their associated advantages while canceling their drawbacks.

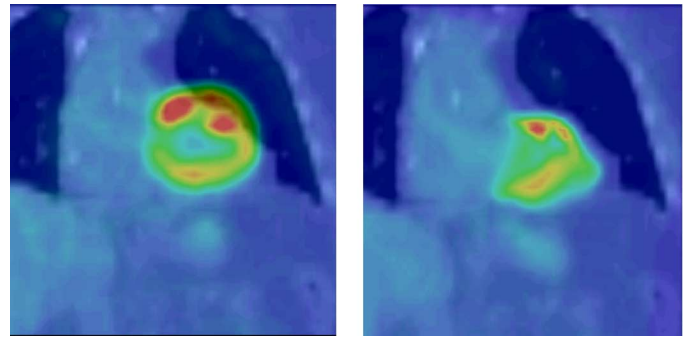


Fig. 9. Case from a combined CT-PET machine in which the proposed methodology corrects a large misalignment in the cardiac region. Two-dimensional coronal slices of the superimposition of the original CT image and the original emission PET image before (left) and after (right) registration.

Segmentation results have proven to be accurate enough for a structure registration procedure to initialize the final grey-level registration stage close to the optimal solution in the region around the available structures.

Results provided by the application of a visual assessment protocol to the pairs of images registered by the proposed methodology prove that we obtain acceptable registration errors for the majority of the targeted thoracic and abdominal structures, except for the stomach. This is due to the absence of this structure in the initialization phase, the strong deformations the stomach undergoes and the presence of close small structures with similar values misleading the intensity-based registration stage.

These promising registration results illustrate the fact that better registration is achieved around structures that have been recognized with the segmentation procedure. Furthermore, the inclusion of the structure registration stage involves a considerable reduction (three times) of the computational cost of the procedure. This allows us to think that the introduction of the proposed methodology in a clinical environment as an additional step in the routine is feasible. Then, a more exhaustive clinical validation of our approach in a larger population could be done. This would confirm the promising results obtained in this work in a relatively limited database or identify cases that the method could potentially fail on. However, a better code optimization and the use of parallelization methods as proposed by Rohlffing *et al.* [63] are still needed to make it possible.

The proposed registration methodology has been also applied to five pairs of images acquired with a PET-CT hybrid system. A substantial improvement has been obtained in one of these sets of images, but we cannot draw any conclusions about it due to the reduced number of processed images.

Current work is focused on the development of a gold standard, using the NCAT phantom [29], [30] and the SIMSET (http://depts.washington.edu/~simset/html/simset_main.html) open-source software, that will allow us to assess in a quantitative way the proposed registration methodology. Furthermore, future work includes a more principled incorporation of tumor-based constraints into the registration procedure aiming at preserving functional information after applying the nonrigid transformation.

ACKNOWLEDGMENT

The authors would like to thank J.-F. Stévenet, P. Briandet, Dr. H. Foehrenbach, Dr. P. Rigo, Dr. Marchandise, Y. Martelli, S. Hammer, the research team of S.H.F.J. in Orsay and the members of Segami Corporation for their contribution to this project. This work has been performed at the TSI Department at the Ecole Nationale Supérieure des Télécommunications, CNRS UMR 5141, Paris, France, in collaboration with SEGAMI.

REFERENCES

- [1] H. Wagner, "Fused image tomography: An integrating force," *Nucl. Med.*, vol. 40, no. 8, pp. 13N–32N, 1999.
- [2] O. Camara, "Non-linear registration of thoracic and abdominal CT and 18-FDG whole-body emission PET images: Methodological study and application in clinical routine," Ph.D. dissertation, Ecole Nationale Supérieure des Télécommunications (ENST), Paris, France, 2003.
- [3] G. Goerres, E. Kamel, T. Heidelberg, M. Schwitter, C. Burger, and G. von Schulthess, "PET-CT image co-registration in the thorax: Influence of respiration," *Eur. J. Nucl. Med.*, vol. 29, no. 3, pp. 1337–1343, 2002.
- [4] T. Beyer, D. Townsend, T. Brun, P. Kinahan, M. Charron, R. Roddy, J. Jerin, J. Young, L. Byars, and R. Nutt, "A combined PET/CT scanner for clinical oncology," *J. Nucl. Med.*, vol. 41, no. 3, pp. 1369–1379, 2000.
- [5] T. Blodgett, T. Beyer, G. Antoch, S. Mueller, L. Freudenberg, and T. Akhurst, "The effect of respiration motion on PET/CT image quality," in *Proc. Conf. Soc. Nucl. Med. (SNM'02)*, 2002, p. 58.
- [6] M. Osman, C. Cohade, and R. Wahl, "Respiratory motion artifacts on PET emission images obtained using CT attenuation correction on PET-CT," in *Proc. Conf. Soc. Nucl. Med. (SNM'02)*, 2002, p. 305.
- [7] M. Osman, C. Cohade, Y. Nakamoto, L. Marshall, J. Leal, and R. Wahl, "Clinically significant inaccurate localization of lesions with PET/CT: Frequency in 300 patients," *J. Nucl. Med.*, vol. 44, pp. 240–243, 2003.
- [8] D. Townsend, J. Carney, J. Yap, and N. Hall, "PET/CT today and tomorrow," *J. Nucl. Med.*, vol. 45, no. 1, pp. 4S–14S, 2003, (Suppl).
- [9] L. Brown, "A survey of image registration techniques," *ACM Comput. Surveys*, vol. 24, no. 4, pp. 325–376, Dec. 1992.
- [10] J. Maintz and M. Viergever, "A survey of medical image registration," *Med. Image Anal.*, vol. 2, no. 1, pp. 1–36, 1998.
- [11] D. Hill, P. Batchelor, M. Holden, and D. Hawkes, "Medical image registration," *Phys. Med. Biol.*, vol. 46, pp. R1–R45, 2001.
- [12] H. Lester and S. Arridge, "A survey of hierarchical non-linear medical image registration," *Pattern Recognit.*, vol. 32, pp. 129–149, 1999.
- [13] B. Zitova and J. Flusser, "Image registration methods: A survey," *Image Vision Comput.*, vol. 21, pp. 977–1000, 2003.
- [14] B. Button, M. Braun, L. Thurfjell, and D. Lau, "Image registration: An essential tool for nuclear medicine," *Eur. J. Nucl. Med.*, vol. 29, pp. 559–577, 2002.
- [15] R. Wahl, L. Quint, R. Cieslak, A. Aisen, R. Koeppe, and C. Meyer, "Anatometabolic tumor imaging: Fusion of FDG PET with CT or MRI to localize foci of increased activity," *J. Nucl. Med.*, vol. 34, pp. 1190–1197, 1993.
- [16] J. Yu, F. Fahey, H. Gage, C. Eades, B. Harkness, C. Pelizzari, and J. Keyes Jr., "Intermodality, retrospective image registration in the thorax," *J. Nucl. Med.*, vol. 36, no. 12, pp. 2333–2338, 1995.
- [17] J. Cai, J. Chu, D. Recine, M. Sharma, C. Nguyen, R. Rodebaugh, V. Saxena, and A. All, "CT and PET lung image registration and fusion in radiotherapy treatment planning using the Chamfer-matching method," *Int. J. Radiation Oncol., Biol., Phys.*, vol. 43, no. 4, pp. 883–891, 1989.
- [18] E. Parsai, K. Ayyangar, R. Dobelbower, and J. Siegel, "Clinical fusion of three-dimensional images using Bremsstrahlung SPECT and CT," *J. Nucl. Med.*, vol. 38, no. 2, pp. 319–324, 1997.
- [19] F. Maes, D. Vandermeulen, G. Marchal, and P. Suetens, "Clinical relevance of fully automated multimodality image registration by maximization of mutual information," in *Proc. Image Registration Workshop*, 1997, pp. 323–330.
- [20] M. Sato, A. E. Hassanien, and M. Nakajima, "Non-linear registration of medical images using Cauchy-Navier splines transformation," in *SPIE Conf. Image Process.*, 1999, pp. 3661–3677.
- [21] C. Meyer, J. Boes, B. Kim, P. Bland, K. Zasadny, P. Kison, K. Koral, K. Frey, and R. Wahl, "Demonstration of accuracy and clinical versatility of mutual information for automatic multimodality image fusion using affine and thin-plate spline warped geometric deformations," *Med. Image Anal.*, vol. 1, pp. 195–206, 1996.
- [22] P. Slomka, D. Dey, C. Przetak, U. Aladl, and R. Baum, "Automated 3-dimensional registration of stand-alone 18F-FDG whole-body PET with CT," *J. Nucl. Med.*, vol. 44, no. 7, pp. 1156–1167, 2003.
- [23] Y. Tai, K. Lin, C. Hoh, S. Huang, and E. Hoffman, "Utilization of 3-D elastic transformation in the registration of chest X-ray CT and whole-body PET," *IEEE Trans. Nucl. Sci.*, vol. 44, no. 4, pp. 1606–1612, Aug. 1997.
- [24] Y. Erdi, K. Rosenzweig, A. Erdi, H. Macapinlac, Y. Hu, L. Braban, J. Humm, O. Squire, C. Chui, S. Larson, and E. Yorke, "Radiotherapy treatment planning for patients with non-small cell lung cancer using positron emission tomography (PET)," *Radiotherapy Oncol.*, vol. 62, no. 1, pp. 51–60, 2002.
- [25] D. Mattes, D. Haynor, H. Vesselle, T. Lewellen, and W. Eubank, "PET-CT image registration in the chest using free-form deformations," *IEEE Trans. Med. Imag.*, vol. 22, no. 1, pp. 120–128, Jan. 2003.
- [26] T. Delzescaux, H. Foehrenbach, and V. Frouin, "A performance study for whole-body helicoidal CT/PET-FDG a posteriori registration using rigid and non-rigid FFD-based methods," *J. Nucl. Med.*, vol. 44, 2003.
- [27] I. Carlsen and H. Wischmann, "Multi-resolution elastic registration of PET-CT images," *Proc. Conf. Soc. Nucl. Med. (SNM'03)*, vol. 44, 2003.
- [28] R. Shekhar, V. Walimbe, S. Raja, V. Zagrodsky, M. Kanvinde, G. Wu, and B. Bydel, "Automated 3-dimensional elastic registration of whole-body PET and CT from separate or combined scanners," *J. Nucl. Med.*, vol. 46, no. 9, pp. 1488–1496, 2005.
- [29] W. Segars, "Development and application of the new dynamic NURBS-based cardiac-torso (NCAT) phantom," Ph.D. dissertation, Dept. Biomed. Eng., Univ. North Carolina, Chapel Hill, 2001.
- [30] W. Segars and B. Tsui, "Study of the efficacy of respiratory gating in myocardial SPECT using the new 4D NCAT phantom," *IEEE Trans. Nucl. Sci.*, vol. 49, no. 3, pp. 675–679, Jun. 2002.
- [31] T. Cootes, G. Edwards, and C. Taylor, "Active appearance models," *IEEE Trans. Pattern Anal. Mach. Intell.*, vol. 23, no. 6, pp. 681–685, 2001.
- [32] D. Rueckert, A. Frangi, and V. T. O. O. A. J. A. Schnabel, "Automatic construction of 3-D statistical deformation models of the brain using nonrigid registration," *IEEE Trans. Med. Imag.*, vol. 22, no. 8, pp. 1014–1025, Aug. 2003.
- [33] Y. Wang and L. Staib, "Physical model-based non-rigid registration incorporating statistical shape information," *Med. Image Anal.*, vol. 4, pp. 7–20, 2000.
- [34] P. Cachier, E. Bardinnet, D. Dormont, X. Pennec, and N. Ayache, "Iconic feature based nonrigid registration: The PASHA algorithm," *Computer Vision Image Understand.*, vol. 89, no. 2–3, pp. 272–298, 2003.
- [35] P. Hellier and C. Barillot, "Coupling dense and landmark-based approaches for nonrigid registration," *IEEE Trans. Med. Imag.*, vol. 22, no. 2, pp. 217–227, Feb. 2003.
- [36] J. Kim, J. Lee, Y. Lee, J. Kim, I. Kim, and S. Kim, "Intensity based affine registration including feature similarity for spatial normalization," *Comput. Biol. Med.*, vol. 32, no. 5, pp. 389–402, 2002.
- [37] T. Liu, D. Shen, and C. Davatzikos, "Deformable registration of cortical structures via hybrid volumetric and surface warping," *NeuroImage*, vol. 22, no. 4, pp. 1790–1801, 2004.
- [38] O. Camara, O. Colliot, and I. Bloch, "Computational modelling of thoracic and abdominal regions by means of spatial relationships," *Real-Time Imag.*, vol. 10, no. 4, pp. 263–273, 2004.
- [39] O. Colliot, O. Camara, R. Dewynter, and I. Bloch, "Description of brain internal structures by means of spatial relations for MR image segmentation," in *Proc. SPIE Conf. Med. Imag.: Image Process.*, 2004, vol. 5370, pp. 444–455.
- [40] F. Maes, "Segmentation and registration of multimodal medical images: From theory, implementation and validation to a useful tool in clinical practice," Ph.D. Dissertation, Katholieke Univ. Leuven, Leuven, Belgium, 1998.
- [41] F. Maes, A. Collignon, D. Vandermeulen, G. Marchal, and P. Suetens, "Multimodality image registration by maximization of mutual information," *IEEE Trans. Med. Imag.*, vol. 16, no. 2, pp. 187–198, Apr. 1997.
- [42] M. Powell, "An efficient method for finding the minimum of a function of several variables without calculating derivatives," *Comput. J.*, vol. 7, pp. 155–162, 1964.
- [43] N. Arad, N. Dyn, D. Riefeld, and Y. Yeshwin, "Image warping by radial basis functions: Application to facial expressions," *Comput. Vision, Graphics Image Process.: Graphical Models Image Process.*, vol. 56, no. 2, pp. 161–172, 1994.

- [44] D. Ruprecht and H. Muller, "Image warping with scattered data interpolation," *IEEE Computer Graphics Appl.*, vol. 15, no. 2, pp. 37–43, Mar. 1995.
- [45] K. Rohr, *Landmark-Based Image Analysis: Using Geometric and Intensity Models*, ser. Computational Imaging and Vision. Norwell, MA: Kluwer, 2001, vol. 21.
- [46] S. Marsland and C. Twining, "Clamped-plate splines and the optimal flow of bounded diffeomorphisms," in *Proc. Leeds Annu. Statist. Res. Workshop*, 2002, pp. 91–95.
- [47] M. Bro-Nielsen and C. Gramkow, "Fast fluid registration of medical images," *Visualization Biomed. Comput. (VBC'96)*, pp. 267–276, 1996.
- [48] G. Christensen, M. Miller, U. Grenander, and M. Vannier, "Individualizing neuroanatomical atlases using a massively parallel computer," *IEEE Computer*, vol. 29, no. 1, pp. 32–38, 1996.
- [49] E. D'Agostino, F. Maes, D. Vandermeulen, and P. Suetens, "A viscous fluid model for multimodal non-rigid image registration using mutual information," in *Proc. Int. Conf. Med. Image Comput. Computer-Assisted Intervention (MICCAI'02)*, 2002, pp. 23–26.
- [50] T. Sederberg and S. Parry, "Free form deformation of solid geometric models," in *Proc. Int. Conf. Comput. Graphics Interactive Techniques (SIGGRAPH'86)*, 1986, vol. 20, pp. 151–160.
- [51] J. Gee, D. Haynor, M. Reivich, and R. Bajcsy, "Finite element approach to warping of brain images," in *Proc. SPIE Conf. Med. Imag.: Image process.*, 1994, vol. 2434, pp. 327–337.
- [52] D. Rueckert, I. Somoda, C. Hayes, D. Hill, M. Leach, and D. Hawkes, "Nonrigid registration using free-form deformations: Applications to breast MR images," *IEEE Trans. Med. Imag.*, vol. 18, no. 8, pp. 712–721, Aug. 1999.
- [53] W. Crum, D. Rueckert, M. Jenkinson, D. Kennedy, and S. Smith, "A framework for detailed objective comparison of non-rigid registration algorithms in neuroimaging," in *Proc. Int. Conf. Med. Image Comput. Computer-Assisted Intervention (MICCAI'04)*, 2004, pp. 679–686.
- [54] O. Camara, W. Crum, J. Schnabel, E. Lewis, M. Schweiger, D. Hill, and N. Fox, "Assessing the quality of Mesh-Warping in normal and abnormal neuroanatomy," in *Med. Image Understand. Anal. (MIUA'05)*, 2005, vol. 1, pp. 79–82.
- [55] A. Frangi, D. Rueckert, J. Schnabel, and W. Niessen, "Automatic construction of multiple-object three-dimensional statistical shape models: Application to cardiac modeling," *IEEE Trans. Med. Imag.*, vol. 21, no. 9, pp. 1151–1166, Sep. 2002.
- [56] O. Camara, G. Delso, and I. Bloch, "Free form deformations guided by gradient vector flow: A surface registration method in thoracic and abdominal PET-CT applications," in *Proc. Workshop Biomed. Image Registration (WBIR'03)*, 2003, pp. 224–233.
- [57] C. Xu and J. Prince, "Generalized gradient vector flow external forces for active contours," *Signal Process., Int. J.*, vol. 71, no. 2, pp. 131–139, Dec. 1998.
- [58] J. Montagnat, "Modèles déformables pour la segmentation et la modélisation d'images médicales 3D et 4D," Ph.D. dissertation, INRIA, Sophia-Antipolis, France, 1999.
- [59] W. Crum, O. Camara, and D. Hill, "Generalised overlap measures for evaluation and validation in medical image analysis," *IEEE Trans. Med. Imag.*, to be published.
- [60] J. Schnabel, C. Tanner, A. Castellano-Smith, A. Degenhard, M. Leach, D. Hose, D. Hill, and D. Hawkes, "Validation of nonrigid image registration using finite-element methods: Application to breast MR images," *IEEE Trans. Med. Imag.*, vol. 22, no. 2, pp. 238–247, Feb. 2003.
- [61] D. Perperidis, M. Lorenzo-Valdes, R. Chandrashekhara, A. Rao, R. Modiaddin, G. Sanchez-Ortiz, and D. Rueckert, "Building a 4D atlas of the cardiac anatomy and motion using MR imaging," in *Proc. Int. Conf. Med. Image Computing Computer-Assisted Intervention (MICCAI'04)*, 2004, pp. 263–273.
- [62] A. Moreno, G. Delso, O. Camara, and I. Bloch, "Non-linear registration between 3-D images including rigid objects: Application to CT and PET lung images with tumors," in *Proc. Workshop Image Registration Deformable Environments (DEFORM'06)*, 2006, pp. 31–40.
- [63] T. Rohlfing and C. Maurer Jr., "Nonrigid image registration in shared-memory multiprocessor environments with application to brains, breasts and bees," *IEEE Trans. Inf. Technol. Biomed.*, vol. 7, no. 1, pp. 16–25, 2003.